Published in final edited form as:
Mol Pharm. 2013 May 6; 10(5): 1683–1694. doi:10.1021/mp300505w.

Nanoparticle Delivered Vascular Disrupting Agents (VDAs): Use of TNF-alpha conjugated Gold Nanoparticles for Multimodal Cancer Therapy

Mithun M. Shenoi[1], **Isabelle Iltis**[2], **Jeunghwan Choi**[3], **Nathan A. Koonce**[5], **Gregory J. Metzger**[2], **Robert J. Griffin**[5], and **John C. Bischof**[1,3,4,*]

[1]Department of Biomedical Engineering, University of Minnesota, Minneapolis, Minnesota

[2]Department of Radiology (CMRR), University of Minnesota, Minneapolis, Minnesota

[3]Department of Mechanical Engineering, University of Minnesota, Minneapolis, Minnesota

[4]Department of Urologic Surgery, University of Minnesota, Minneapolis, Minnesota

[5]Department of Radiation Oncology, University of Arkansas for Medical Sciences, Little Rock, Arkansas

Abstract

Surgery, radiation and chemotherapy remain the mainstay of current cancer therapy. However, treatment failure persists due to the inability to achieve complete local control of the tumor and curtail metastatic spread. Vascular disrupting agents (VDAs) are a class of promising systemic agents that are known to synergistically enhance radiation, chemotherapy or thermal treatments of solid tumors. Unfortunately, there is still an unmet need for VDAs with more favorable safety profiles and fewer side effects. Recent work has demonstrated that conjugating VDAs to other molecules (polyethylene glycol, CNGRCG peptide) or nanoparticles (liposomes, gold) can reduce toxicity of one prominent VDA (tumor necrosis factor alpha, TNF-α). In this report, we show the potential of a gold conjugated TNF-α nanoparticle (NP-TNF) to improve multimodal cancer therapies with VDAs. In a dorsal skin fold and hindlimb murine xenograft model of prostate cancer, we found that NP-TNF disrupts endothelial barrier function and induces a significant increase in vascular permeability within the first 1–2 hours followed by a dramatic 80% drop in perfusion 2–6 hours after systemic administration. We also demonstrate that the tumor response to the nanoparticle can be verified using dynamic contrast-enhanced magnetic resonance imaging (MRI), a technique in clinical use. Additionally, multimodal treatment with thermal therapies at the perfusion nadir in the sub- and supra- physiological temperature regimes increases tumor volumetric destruction by over 60% and leads to significant tumor growth delays compared to thermal therapy alone. Lastly, NP-TNF was found to enhance thermal therapy in the absence of neutrophil recruitment, suggesting that immune/inflammatory regulation is not central to its power as part of a multimodal approach. Our data demonstrate the potential of nanoparticle-conjugated VDAs to significantly improve cancer therapy by preconditioning tumor vasculature to a secondary insult in a targeted manner. We anticipate our work to direct investigations into more

*Corresponding Author: John C. Bischof, Professor, Department of Mechanical Engineering, University of Minnesota, 111 Church Street SE, Minneapolis, MN 55455, USA, Phone: +1-612-625-5513, Fax: +1-612-625-4344, bischof@umn.edu.

The authors declare no competing financial interests.

SUPPLEMENTARY INFORMATION

DSFC histology following multimodal therapy and neutrophil depletion experimental data. This material is available free of charge via the Internet at http://pubs.acs.org.

potent tumor vasculature specific combinations of VDAs and nanoparticles with the goal of transitioning optimal regimens into clinical trials.

Keywords

vascular disrupting agent; gold nanoparticles; TNF-alpha; DCE-MRI; thermal therapy; cancer; CYT-6091

INTRODUCTION

Multimodal approaches to controlling solid tumors with radiation, chemotherapy and surgery are now used on high-grade cancer, the most life threatening form of the disease [1, 2]. Nevertheless, the lack of definitive improvements in tumor control begs further development. One promising approach involves the use of vascular disruptive agents (VDAs) with focal and systemic multimodal treatments [3]. For instance, numerous pre-clinical studies have demonstrated the efficacy of combining VDAs with chemotherapy, radiation, and focal thermal therapies and many of these approaches are now under clinical evaluation [4, 5]. Nevertheless, data from the clinical trials show minimal improvement in the combination of VDAs with frontline therapies, i.e. chemotherapy and radiation, and demonstrated dose limiting toxicities including systemic hypotension, cardiotoxicity, reversible ataxia, vasovagal syncope, motor neuropathy, reversible confusion, tremor, slurred speech and visual disturbance [3, 6–10]. Hence, further work to realize the promise of VDAs for multimodal treatments through increased efficacy and reduction in toxicity is needed.

One approach to improving the clinical use of VDAs is to re-package them with other molecules and/or using nanoparticle constructs to improve tumor specific delivery and effect. As an example, one of the most prominent VDAs, tumor necrosis factor alpha (TNF-α), was originally plagued by dose limiting toxicities, but non-systemic delivery in the form of isolated limb perfusion (ILP) has been shown to be highly efficacious without dose limiting toxicity when used with multimodal approaches [11, 12]. Several approaches have been tested previously to selectively deliver TNF-α to solid tumors with the goal of improving the antitumor response and decreasing toxicity (Table 1). Thus, recent work has re-focused on delivery of TNF-α in liposomal form (Preclinical), NGR- TNF-α (Phase 3), and on a gold nanoparticle NP-TNF (Phase 1). In the case of NP-TNF a clinical trial demonstrated 3-fold increase in maximum tolerated dose of TNF-α suggesting that this nanoparticle formulation may be effective in future multimodal treatments [13].

In this report, we show the potential of the TNF-α gold nanoparticle (NP-TNF) to improve VDA tumor specific action in combination with locally applied thermal therapy in prostate cancer. Our results demonstrate: (1) a mechanism of action for and physiological response to NP-TNF by the LNCaP prostate tumor model, (2) the ability to image this response with contrast MRI, and (3) demonstration of significant enhancement in the absence of neutrophil recruitment suggesting that this enhancement is related to the direct action of NP-TNF on vascular stability and can occur without a major acute inflammatory response.

MATERIALS AND METHODS

Tumor Growth (DSFC and hindlimb preparations)

All animal protocols were reviewed and approved by the University of Minnesota and the University of Arkansas Medical Sciences Institutional Animal Care and Use Committee. 6–8 week old athymic male NU/J mice were obtained from the Jackson Laboratory (Bar

Harbor, ME). Tumors were either grown in a dorsal skin fold chamber (DSFC) or the hindlimb of the animals as previously described [5, 14, 15]. Briefly, 1–2 million LNCaP Pro 5 cells suspended in 100 μl Matrigel (BD Biosciences, San Jose, CA) and diluted 3:1 in serum-free medium were inoculated into the DSFC chamber window on both day 0 and day 4 following chamber implantation [14, 15]. Thermal therapy experiments were performed between day 12 and 14 following DSFC implantation, when tumor cells were found to cover the entire chamber window as previously reported [5, 14, 15]. In the hindlimb, 5 million LNCaP Pro 5 cells suspended in 100 μl Matrigel (BD Biosciences, San Jose, CA) that had been diluted 3:1 in serum-free medium were injected subcutaneously. All hindlimb experiments were performed after 4 to 5 weeks, when the tumors reached a diameter of 6 to 8 mm. Chamber implantation and inoculation in the hindlimb were performed under anesthesia using an i.p. injection of ketamine (100 mg/kg) and xylazine (10 mg/kg).

Nanoparticle Administration

The gold nanoparticle NP-TNF used in this study was manufactured as the drug CYT-6091 (CytImmune Sciences, Inc., Rockville, MD, USA). 5 μg of TNF-α in nanoparticle form was diluted in 100 μl sterile water and injected via tail vein into the mice 4 hours prior to thermal therapy. In experiments with control nanoparticles, AuPEG (PEGylated colloidal gold nanoparticle without TNF-α, CytImmune Sciences, Inc.) were administered in the same manner at an equivalent dose to injected NP-TNF based on total surface area of injected particles. The 5 μg TNF-α dose and 4 hour time period were chosen based on previous work with NP-TNF [14, 16].

Assessment of Tumor Vasculature

DSFC Tumor Vascular Permeability—TNF-α induced vascular permeability was assessed as previously described [17]. One hour after i.v. administration of NP-TNF (5 μg of TNF-α), 0.04 ml of 20 mg/ml 70-kDa TxRed-labeled dextran was injected into the tail vein of each animal. Images of the DSFC tumor vasculature were obtained at time 0, 15 minutes and 30 minutes after TxRed-dextran injection using an Olympus IX71fluorescent microscope (Olympus Inc., Tokyo, Japan) equipped with a 10X objective and an Olympus DP72. Images were analyzed using ImageJ software (NIH, Bethesda, MD, USA).

Hindlimb Tumor Perfusion—At specific time points after NP-TNF injection, animals were anesthetized by an i.p. injection of ketamine and xylazine at 100 and 10 mg/kg, respectively, and the heart was exposed via a median sternotomy. 10^6 colored microspheres (10 μm diameter, E-Z-Trac Ultraspheres, E-Z-Trac Inc., Los Angeles, CA) were injected into the left ventricle under direct visualization. The anesthetized mice were sacrificed 2 minutes after microsphere injection [18, 19]. Tumors were harvested, weighed, and microbeads were isolated and counted according to the manufacturer's instructions.

Histology and Immunohistochemistry—Animals were sacrificed 4 hours after NP-TNF injection or at day 3 post DSFC cryosurgery immediately after vascular imaging. The entire tumor tissue attached to the chamber was fixed in 10% buffered formalin (Sigma, St. Louis, MO), embedded in paraffin, and sectioned at 4 μm intervals.

Tumor Accumulation of Nanoparticles—For visualizing nanoparticle accumulation within the tumor, deparaffinized sections were washed in DI water, 0.02 M sodium citrate (pH 3.5), and DI water in that order. Sections were silver enhanced using LI Silver® (Nanoprobes, Inc., Yaphank, NY) and counter stained with hematoxylin and eosin (H&E).

Quantification of Inflammatory Cell (Neutrophil) Recruitment—Immunohistochemistry detecting myeloperoxidase, MPO, (1:2000; A0398, DAKO,

Glostrup, Denmark) was performed on deparaffinized sections using the Rabbit on Rodent-HRP polymer kit (BioCare Medical, Concord, CA, USA) followed by 3,3′-Diaminobenzidine (DAB) chromagen staining. Tissue sections were counterstained with hematoxylin according to standard protocols, scanned using Aperio ScanScope (Axiovision Technologies, Toronto, Ontario, Canada) and analyzed using Aperio ImageScope software. On tumors obtained Day 3 post cryosurgery, digital annotation regions were applied around the zones of central necrosis and the inflammatory bands to quantify the respective areas on each section. The number of MPO positive cells in 5 representative regions within each histological zone was counted using light microscopy at 40X magnification.

Quantification of Fibrin Deposition—Immunohistochemistry detecting fibrinogen (1:2000; A0080, DAKO) was performed on deparaffinized sections using the Rabbit on Rodent-HRP polymer kit (BioCare Medical) followed by 3,3′-Diaminobenzidine (DAB) chromagen staining. Sections were counterstained, scanned and analyzed as described above. For quantification of fibrinogen staining intensity, digital annotation regions were applied to representative areas of each tumor section and pixels that exceeded threshold limits were quantified (as a % of total) using Color Deconvolution v9 algorithm (Aperio, Vista, CA).

Tumor Microvessel Analysis—Immunohistochemistry detecting endothelial cell marker CD31 (1:25, Clone: SZ31, Dianova, Hamburg, Germany) was performed on deparaffinized sections using Rat on Mouse AP-Polymer kit, BioCare Medical) followed by fast red staining (Vulcan Fast Red chromagen kit 2, BioCare Medical). Sections were counterstained, scanned and analyzed as described above. Digital annotation regions were applied in representative areas of each tumor section and Microvessel analysis v1 algorithm (Aperio, Vista, CA) was applied to count the number of vessels.

MRI Imaging of Vascular Permeability & Perfusion

Dynamic Contrast Enhanced Magnetic Resonance Imaging (DCE-MRI) was performed on mice bearing hindlimb LNCaP tumors. Mice were imaged twice. The first scanning session was performed before injection of NP-TNF (Pre-NP-TNF) to assess the tumor at baseline. After allowing the mice to recover for 48 hours, mice were scanned a second time 4 hours after NP-TNF injection (Post-NP-TNF). During the imaging experiment, mice were anesthetized with isoflurane in O_2/N_2O (50/50), and Gadolinium-DTPA (Gd, 0.6 mmol/kg i.p.) was used as the contrast agent. An i.p. injection of Gd was used in this study as the typical use of the tail vein for intravenous injections typically resulted in failed contrast delivery post NP-TNF. Animals were scanned using an RF volume coil (Millipede, Agilent, Palo Alto) at a 9.4T magnet equipped with a Varian console. A multislice gradient echo sequence was acquired at multiple flip angles (5 – 40°) to calculate T_1 maps prior to Gd injection (field-of-view 35 × 35 mm, matrix size = 128 × 128, TE = 1.43 ms, TR = 35 ms, 10 slices, 1 mm thickness, 8 averages). The same sequence, at a flip angle of 30°, was used after Gd injection to acquire DCE-MRI data with a temporal resolution of 66 s for a total acquisition time of approximately 90 min. Contrast enhancement curves from the DCE-MRI acquisitions were obtained in tumor regions both Pre- and Post- NP-TNF administration for all mice using a DICOM viewing software (OsiriX) [20]. The mean and standard error of the percent signal enhancement was determine over the time course of the DCE-MRI studies for all tumors regions from all mice in order to compare the differences in contrast dynamics Pre- and Post- NP-TNF administration.

For individual mice, parametric maps showing the integrated area under the Gd concentration-time (AUGC) curves were generated to visualize the spatial accumulation of Gd in both the tumors and skeletal muscle. The time course data were first converted to

concentration using the the pre-contrast T_1 maps [2122] followed by integration over the entire time coarse on a pixel-wise basis in IDL (Exelis Visual Information Solutions, Boulder, CO, USA). Regions of interest determined on the corresponding grey-scale images and transferred to the AUGC maps were used to assess contrast uptake differences in both tumor and muscle. For the muscle regions, large vessels and bones were avoided.

Multimodal Focal Thermal Therapy

Dorsal Skin Fold Chamber (DSFC) Thermal Therapy—Briefly, animals were anesthetized, DSFC windows were removed and cryosurgery or thermal therapy was imposed on the tumor. For cryosurgery, a 1 mm diameter brass extension tip fitted to a 5 mm cryoprobe (Endocare, Irvine, CA) was inserted into the center of the DSFC for 55 seconds (to attain tip temperatures of −85°C) followed by passive thawing at room temperature. The tumor temperature was monitored throughout the procedure using an infrared camera ThermoVision (FLIR Systems, Boston, USA) and thermocouples placed at 2, 3 and 4 mm radial positions around the DSFC center [14, 15, 23]. For high temperature thermal therapy, heating was initiated from the center of the DSFC using a 1 mm diameter brass extension tip fitted to a temperature controlled soldering iron tip (RadioShack Digital Soldering Station 64–053, RadioShack, Fort Worth, TX, USA). A tip temperature of 80°C was obtained for these experiments. This allowed a radial heating front to develop from the center of the DSFC tissue and the temperature to be monitored using infrared thermography and thermocouples similar to the cryosurgery procedure. The soldering iron was switched off when the thermocouple positioned 2 mm away from the center of the DSFC reached 45°C and the tissue was allowed to passively cool to room temperature. Total heating time was less than 10 min.

Hindlimb Thermal Therapy—Cryosurgery was performed using a cryosurgical system (Endocare, Inc., Irvine, CA, USA), as described previously, with a 1 mm probe tip modification on a 3 mm tip cryoprobe [14]. A small incision was first made in the center of the hindlimb tumor with a 21-gauge needle to allow insertion of the probe tip without deformation of the tumor. Freezing (at tip temperatures of −85°C) was performed conservatively under infrared thermographic guidance until the 0°C isotherm reached the visible edge of the tumor. The tumor was then passively thawed to room temperature. For high-temperature thermal therapy, the 1 mm diameter brass extension tip was fitted to a temperature controlled soldering iron tip (RadioShack Digital Soldering Station 64–053, RadioShack, Fortworth, TX, USA) and inserted into the tumor after a small incision was made with a 21-gauge needle. The soldering iron was switched on at the lowest temperature (150°C) setting and the tumor was heated conservatively under infrared thermographic guidance until the 40°C isotherm reached the visible edge of the tumor. The tip was then removed and the tumor was passively cooled to room temperature.

Treatment Outcome Measures

DSFC Tumor Vascular Stasis—On days 1 and 3 following thermal therapy (with or without nanoparticle administration), 0.1 ml of 10 mg/ml 70-kDa FITC-labeled dextran (Sigma, St. Louis, MO) was injected into the tail vein of each animal. Intravital imaging of tumor vasculature in the DSFC was performed using a Nikon inverted fluorescent microscope equipped with a 20× objective (Nikon, Melville, NY) and silicon intensified transmission camera (Hamamatsu, Bridgewater, NJ) as previously described [14, 15, 23]. The average radius at which patent blood vessels with blood flow were clearly visible defined the region of vascular stasis and was measured at four perpendicular radial directions relative to the chamber center. The stasis area was calculated as $\pi \times (\text{average radius})^2$. Vascular stasis areas measured in this manner were compared with histological measurement of tumor necrosis areas (Supplementary Information, Figure S1).

Hindlimb Tumor Growth Delay—Baseline tumor size in the hindlimb was measured prior to thermal therapy (cryosurgery or HTT). Tumor growth is reported relative to the size prior to thermal therapy. Tumor volumes were measured every 3 days for 30 days after thermal therapy. Tumor dimensions were measured using calipers and volumes were calculated and reported as 0.53 × width × length × height [14, 24].

Neutrophil Depletion

24 hours prior to NP-TNF injection, mice were injected intraperitoneally with 150 μg purified RB6-8C5 rat monoclonal antibody (BD Pharmingen, Rockville, MD) in order to systemically deplete granulocytes, especially neutrophils [25]. Cryosurgery was performed 4 hours after NP-TNF injection as described above. Systemic depletion was confirmed in a separate set of mice injected with the same dose of RB6-8C5 antibody. About 60–80 μl of blood was collected by facial vein puncture from each mouse on day 1, 2, 3 and 4 after antibody injection and analyzed using an automated cell counter to demonstrate neutrophil depletion (Hemavet 950, Drew Scientific, Oxford, Connecticut, USA).

Statistics

Statistical significance was determined using the wilcoxon test in R statistical software [26]. If the difference was at the level of $p<0.05$, it was determined significant. Otherwise, the difference between two measurements was not significant, i.e., $p>0.05$. Data are represented as mean ± SE.

RESULTS

Systemic administration of NP-TNF induces vascular disruptive events in LNCaP tumor

Figure 1 demonstrates vascular permeability increase and perfusion drop due to NP-TNF delivery to the tumor vasculature. For instance, fluorescence imaging in the DSFC demonstrated a robust vascular leak of fluorescent dye from the tumor vasculature 1–1.5 hours after systemic administration of NP-TNF (5 μg TNF-α) (Figure 1A). As expected, the intravascular fluorescence intensity of imaged tumor vessels diminished over time while extravascular fluorescence increased. Further, in the hindlimb model 4 hours after systemic injection of NP-TNF (5 μg TNF-α), tumor perfusion dropped to 19.8 ± 8.2% of controls ($p = 0.002$) (Figure 1B) consistent with previous results for VDAs and NP-TNF [16, 27]. This drop in perfusion persisted up to 6 hours (16.1 ± 6.1%) after nanoparticle injection. Increasing the dose of NP-TNF to 10 μg TNF-α, did not drop tumor perfusion further at 6 hours (19.9 ± 6.6%). As expected, partial recovery of tumor perfusion was obtained at 24 hours (59.2 ± 14.7%). The perfusion drop induced by NP-TNF at 4 hours was accompanied by enhanced fibrinogen staining in DSFC tumors (Figure 1C). These results are in agreement with regions of complete vascular stasis observed under light microscope within DSFC LNCaP tumors 4 hours after NP-TNF systemic administration (data not shown).

Tumor localization of NP-TNF nanoparticles 4 hours after i.v. injection was confirmed on H&E and silver co-stained sections for DSFC (Figure 1D) and hindlimb (data not shown) LNCaP tumors. Nanoparticles were found in the vascular and perivascular regions with little or no extravasation into the interstitial space. CD31 immuno-staining and silver co-staining of these tumors confirmed that the nanoparticles were in close proximity and interacting with the tumor endothelium (Figure 1E). Consistent with an endothelial response, CD31 stained tumor sections showed dilated microvessels in the NP-TNF treated group compared to control (Figure 1F, G). A microvessel analysis algorithm was used to quantify the change in tumor vessel size 4 hours after systemic administration of NP-TNF. Over 5000 vessels were analyzed in each group and a significant increase in vessel lumen area was obtained in the NP-TNF group (41.10 ± 0.94 μm^2) compared to control (36.03 ± 0.94 μm^2, $p<0.001$).

These results are similar to previous results reported by our group, i.e. TNF-α increases diameter of tumor blood vessels [5].

DCE-MRI detects NP-TNF induced vascular changes in LNCaP tumors

Figure 2A shows an axial view of a typical mouse bearing LNCaP tumors after Gd injection and Figure 2B shows the percent change in signal intensity following Gd injection averaged over all tumors from both the Pre-NP-TNF and Post-NP-TNF experiments. In the tumor, contrast uptake is enhanced after NP-TNF administration (Post-NP-TNF) compared to the uptake measured before NP-TNF administration (Pre-NP-TNF). A similar effect was also observed in the muscle, however to a lesser degree (data not shown). Figure 2C and 2D shows AUGC maps Pre- and Post- NP-TNF, respectively, where the accumulation of Gd is 4 times higher in the Post-NP-TNF tumor. Interestingly, the accumulation of Gd also increased in muscle Post-NP-TNF, however the percent AUGC increase was 3 fold higher in the tumor and less than 2-fold higher in the muscle.

Combination of NP-TNF with thermal therapy increases LNCaP tumor destruction compared to thermal therapy alone

To demonstrate the potential of NP-TNF in multimodal cancer treatment, we injected mice with the nanoparticle 4 hours prior to two different types of thermal therapy – cryosurgery and high-temperature thermal therapy (HTT) – in DSFC (Figure 3A) and hindlimb LNCaP tumor models. In the DSFC, mice injected with NP-TNF yielded an 80% increase in tumor injury (vascular stasis) compared to cryosurgery alone and AuPEG + cryosurgery treated groups at Day 1 and Day 3 (Figure 3B). NP-TNF administration reduced the thermal threshold of injury from −8.0 ± 1.9°C and −7.3 ± 2.0°C, in the control and AuPEG groups respectively, to 8.3 ± 1.0°C (Figure 3B). This enhancement of cryosurgery by combination with NP-TNF was also demonstrated in LNCaP tumors grown subcutaneously in the hindlimb. Specifically, in mice injected with NP-TNF prior to cryosurgery, the volume of tumors regressed significantly to 50 ± 5.6% of the starting volume within 6 days of treatment (Figure 3C). The volume of tumors in mice treated with AuPEG + cryosurgery regressed to a lesser extent to 73 ± 8.9% whereas no regression was seen in cryosurgery alone group. At Day 30 after cryosurgery, the relative tumor volumes of cryosurgery alone and AuPEG + cryosurgery alone groups were not statistically different from each other. NP-TNF combined with cryosurgery group had the lowest relative tumor volumes.

Similar to cryosurgery, thermal injury by HTT in DSFC LNCaP tumors was also assessed by vascular stasis measurements. Thermal response during the course of HTT was characterized within the DSFC (data not shown) and temperatures >50°C were obtained in the tumor within 2 mm of the probe tip. Mice injected with NP-TNF yielded a 61% increase in tumor injury (vascular stasis) compared to HTT alone and AuPEG + HTT treated groups at Day 1 and Day 3. As in cryosurgery, NP-TNF administration reduced the thermal threshold of injury from 40 ± 1.2°C and 42 ± 1.0°C, in the HHT alone and AuPEG + HTT groups respectively, to 36 ± 1.0°C in the NP-TNF group (Figure 3B). The same enhanced treatment response trend was observed in hindlimb LNCaP tumors. Over the course of 30 days following treatment, the NP-TNF + HTT treated mice exhibited a much greater tumor growth delay compared to the other groups (Figure 3C). At Day 30 after treatment, the relative tumor volumes of control, HTT alone and AuPEG + HTT groups were not statistically different from each other. However, the NP-TNF + HTT relative tumor volumes were significantly lower than the other groups. No animal deaths occured in any treatment group.

Vascular disruptive events of NP-TNF are independent of the neutrophil inflammatory response within tumors

Based on our previously published results, we hypothesized that increased recruitment of neutrophils is essential for the enhanced cryosurgical lesion due to nanoparticle preconditioning [15, 23]. To elucidate the role of the inflammatory cell response, we first investigated the recruitment of neutrophils to DSFC LNCaP tumor tissue during the 4 hour period after NP-TNF administration by myeloperoxidase staining. No significant differences were observed between neutrophil numbers in control tumors compared to tumors in mice injected with AuPEG or NP-TNF after 4 hours (Figure S2A). Next, we tested the functional role for neutrophils by systemic depletion of neutrophils prior to multimodal therapy with NP-TNF and cryosurgery. Systemically circulating neutrophils were diminished to 11.2 ± 3.5% of baseline values at 24 hours after i.p. injection of anti-Ly6G (RB6-8C5) antibody (Figure S2B). Cryosurgery was then performed in neutrophil-depleted mice 4 hours after NP-TNF injection.

First, we analyzed neutrophil recruitment in the cryosurgical lesion at Day 3 following DSFC LNCaP tumor cryosurgery (Figures 4A–C). Tumors in mice treated with cryosurgery alone showed the characteristic histologic zones associated with cryosurgical injury i.e. a central necrotic zone adjacent and concentric to the cryoprobe tract surrounded by a band of inflammatory infiltrate and viable tumor tissue (Figure 4A). In mice treated with NP-TNF and cryosurgery the lesion was markedly different with a large central necrotic zone surrounded by a thin band of inflammatory infiltrate and viable tumor tissue (Figure 4B). The number of neutrophils present in the inflammatory band in this group was not statistically different compared to the cryosurgery alone group. In mice treated with NP-TNF and cryosurgery following systemic neutrophil depletion, a similar trend was seen with a large central necrotic zone surrounding the cryoprobe tract but with only a thin inflammatory band at the boundary of viable tumor tissue (Figure 4C). Finally, we demonstrated that systemic neutrophil depletion did not reduce NP-TNF mediated enhancement of cryosurgical injury (vascular stasis) at Day 1 or Day 3 after therapy (Figure 4D). This was confirmed by measuring the histological area of necrosis which correlated well with the vascular stasis area measurements (Figure 4D).

DISCUSSION

With several vascular disruptive agents (VDAs) entering Phase 2/3 clinical trials in recent times there is tremendous interest within the research and clinical community in understanding their interaction with traditional cancer therapies – surgery, chemotherapy and radiation - in order to develop new multimodal therapies [28]. In addition, several nanoparticles delivering small molecule chemotherapeutics, proteins and nucleic acids have received FDA approval or are in clinical trials for cancer therapy [29]. A limited number of these nanoparticle formulations are being investigated in combination with thermal therapies [30]. Promisingly, Phase 2 and 3 clinical trials are in progress to demonstrate clinical efficacy of multimodal therapy using thermally sensitive liposomes containing doxorubicin (ThermoDox®) and radiofrequency ablation for the treatment of hepatocellular carcinoma and colorectal liver metastases [31]. NP-TNF (i.e. CYT-6091), the TNF-α conjugated gold nanoparticle that we have used in our experiments is one of the first VDA conjugated nanoparticles to have completed a Phase 1 clinical trial [13].

The mechanism of nanoparticle preconditioning by VDA conjugated gold nanoparticles rely upon the size, PEG coating, and VDA ligand as recently reviewed [30]. For instance, smaller 20 nm PEGylated gold nanoparticles will passively load (enhanced permeability and retention effect) and diffuse more deeply into the tumor interstitium versus larger 100 nm nanoparticles) as recently shown [32]. Interestingly, the presence of the VDA appears to arrest

this diffusion and localizes the nanoparticle in and around the tumor endothelial cells as shown here by CD31 and silver co-staining and previously in histology [33]. Localization of the nanoparticles to the tumor endothelium is expected as TNF-α present on NP-TNF nanoparticles acts as a ligand for TNFR1 receptors present in abundance on tumor endothelial cells [34]. Classical VDA response includes profound vascular disruption in tumors including vascular permeability changes, perfusion drop, endothelial injury and stasis [35]. These changes are so powerfully anti-tumor that despite systemic toxicity, TNF-α is still used in isolated limb perfusion to treat various cancers [12]. Farma et al have previously demonstrated that intravenously administered NP-TNF induces vascular hyperpermeability in vivo in a TNF-α-sensitive MC38 tumor cell line [17]. In this work, we found that NP-TNF leads to many of the same classic VDA responses such as disruption of endothelial barrier function and a concurrent significant increase in vascular permeability within the first 1–2 hours followed by a dramatic 80% drop in perfusion 2–6 hours after systemic administration. In addition, we have shown an increase in the deposition of fibrinogen 4 hours after the injection of NP-TNF suggesting optimal conditions have been created to augment or sustain vascular stasis through thrombosis. Furthermore, NP-TNF alone has been shown previously to increase endothelial cell death alone (another hallmark of a VDA response) [16, 23]. Finally, all of these VDA related mechanisms, which are enhanced by nanoparticle delivery, are occurring within the context of reduced systemic toxicity as indicated by a greater than three-fold increase in maximum tolerated dose in a recent clinical trial [13].

Due to the importance of establishing VDA nanoparticle response non-invasively and for timing subsequent multimodal therapies that leverage the pre-conditioned vascular environment we demonstrate here for the first time that nanoparticle preconditioning of the vasculature can be measured using an MRI approach available clinically. Endothelial barrier disruption and tumor hyperpermeability evidenced by fluorescence imaging in DSFC tumor is demonstrated by MRI in the hindlimb model with the total contrast uptake being much higher in the tumors after injection of NP-TNF. Our data also appear to capture the decreased perfusion in NP-TNF treated tumors. For instance, slower uptake of contrast in the early phase of the dynamic contrast enhancement curves (Figure 2B, between 10 to 20 minutes) likely reflects the difference in tumor perfusion. Further studies are warranted to confirm this effect. Interestingly, despite the reduced toxicity of NP-TNF demonstrated in previous studies, the contrast enhancement data using MRI revealed that there is a non-negligible systemic effect, at least in muscle. We performed these studies on a dedicated, ultrahigh field (9.4T) research system, therefore potentially benefitting from a higher signal-to-noise ratio compared to clinical field strengths, however we anticipate that the VDA effects will be easily detected at clinical fields of 1.5T and 3.0T [36]. Because of the tumor model and contrast injection strategies used in this study, the contrast kinetics observed in mice (occurring over 90 minutes) are strikingly slower than in the human prostate (occurring over 5 minutes). That is, a standard clinical DCE-MRI imaging protocol with a duration of 5 minutes will most likely be a sensitive and practical method to evaluate the effectiveness of NP-TNF administration in clinical trials. The ability to spatially resolve the effects NP-TNF with DCE-MRI would be important to optimally design and employ patient-tailored therapeutic strategies as well as monitor off-target effects away from the tumor[36].

The multimodal data presented here show that NP-TNF preconditioning of the vasculature can enhance cryosurgery and high-temperature thermal therapy in a preclinical prostate cancer model in both 2D DSFC and 3D hindlimb tumor. We also observed that the gold nanoparticle without VDA (AuPEG) did not affect the thermal therapy outcome implying that the postulated antiangiogenic properties of gold nanoparticles do not play a role in the timeframes used in this study [37]. Importantly, there were no deaths in any of the animal groups using NP-TNF although previous work with native TNF administration at the same

dose followed by thermal therapy is lethal to a large percentage of the animals as previously shown [14, 24]. Thus, thermal thresholds of injury were reduced in a safer manner for both heat and cold thermal therapies by VDA conjugated nanoparticle delivery vs. VDA alone. In the 2D DSFC model, NP-TNF preconditioning led to an 80% increase in the treated tumor volume by cryosurgery while a 61% increase was obtained with HTT. Importantly, the thermal thresholds measured within the DSFC with and without NP-TNF should be considered in a relative rather than absolute sense since tumors in the DSFC are destroyed more easily than hindlimb or in vitro tumors [38–42]. Thus, a further test with the hindlimb system was undertaken and despite the conservative thermal threshold protocols (edge of tumor = iceball edge or 40°C for HTT) a significant therapeutic benefit (tumor growth delay) was still realized.

Finally, our data demonstrate that the acute inflammatory response (i.e. neutrophil recruitment) does not influence nanoparticle enhancement of thermal destruction of the tumor. The role of TNF-α in recruiting leukocytes to the tumor endothelium is well established [43]. In addition, the role of inflammatory cells especially neutrophils in determining the maximum extent of the cryosurgical lesion is well documented [44]. Previous data from our lab showed an increased recruitment of inflammatory infiltrate into DSFC LNCaP tumors 4 hours after topical administration of 200 ng native TNF-α [15]. This was accompanied by significantly higher recruitment of neutrophils in the inflammatory zone of the Day 3 cryolesion with TNF-α plus cryosurgery compared to cryosurgery alone [15]. However, our experiments show that systemically delivered NP-TNF neither induces an increased recruitment of inflammatory infiltrate to the tumor after 4 hours nor in the Day 3 cryolesion following multimodal therapy. This led to the question whether neutrophils were merely “bystanders” in our previous experiments with topical administration of native TNF-α having played no functional role in determining the extent of the cryolesion. Multimodal therapy following systemic depletion of neutrophils supported this theory as the size of the cryolesion was unaffected by the reduction in circulating neutrophil numbers. The reason for these differences in responses of native TNF-α and NP-TNF to neutrophil recruitment is unclear. We speculate that this is likely due to the differences in delivery method (topical versus intravenous) and the effective dose of TNF-α interacting with the tumor tissue i.e. 200 ng of native TNF-α administered topically yields a much higher effective local dose of TNF-α when compared to 5 μg of nanoparticle bound TNF-α delivered systemically. Of note, our results are focused on the acute phase of the inflammatory response and do not account for the role of macrophages and other immune cells that could potentially play an important role in determining the extent of the thermal lesion [45].

CONCLUSIONS

In summary, we have demonstrated the ability of a gold nanoparticle conjugated VDA (TNF-α) to significantly enhance both cryotherapy and hyperthermic therapy without evidence of systemic toxicity measured here as mortality. We also characterized the mechanisms responsible for these improved outcomes as related to tumor-specific vascular disruptive effects of the nanoparticle, i.e. increase in vascular permeability within the first 1–2 hours followed by a significant drop in perfusion 2–6 hours after systemic administration. In addition, we showed the ability of DCE-MRI to register these vascular changes induced within the tumor. Lastly, in contrast to locally administered VDAs, our systemically delivered nanoparticle data suggests that neutrophil dependent inflammatory response is not important in multimodal thermal therapy enhancement with NP-TNF.

Supplementary Material

Refer to Web version on PubMed Central for supplementary material.

Acknowledgments

The authors acknowledge funding from NIH 2R01 CA075284 (JCB), a Distinguished McKnight University Professorship (JCB), a Grant-in-Aid Seed Grant (JCB) and an AHC Seed Grant (GJM). The authors wish to also thank Dr. Steve Schmechel for useful discussions and guidance for the histology work. We thank Colleen Forster and Jonathan Henriksen for technical support at BioNet facilities (University of Minnesota, Minneapolis, MN). BioNet facilities are supported by NIH grants P30 CA77598 (D. Yee), P50 CA101955 (D. Buchsbaum) and KL2 RR033182 (B. Blazar), and the University of Minnesota Academic Health Center. We thank John Oja for technical support at University Imaging Centers (University of Minnesota, Minneapolis, MN). NP-TNF (CYT-6091) nanoparticles were a gift from CytImmune Sciences (Rockville, MD). We thank Krista Walkowiak DVM, Emily Colonna and Manda Vollmers for assistance with animal care.

Abbreviations

DSFC	dorsal skin fold chamber
Gd	Gadolinium-DTPA
HTT	high-temperature thermal therapy
NP-TNF	tumor necrosis factor alpha tagged gold nanoparticle
TNF-α	tumor necrosis factor alpha
VDA	vascular disrupting agent

References

1. Chang SS. Management of high risk metastatic prostate cancer: defining risk at the time of initial treatment failure. J Urol. 2006; 176(6 Pt 2):S57–60. discussion S55–6. [PubMed: 17084169]
2. D'Amico A. Global update on defining and treating high-risk localized prostate cancer with leuprorelin: a USA perspective--identifying men at diagnosis who are at high risk of prostate cancer death after surgery or radiation therapy. BJU Int. 2007; 99(Suppl 1):13–6. discussion 17–8. [PubMed: 17229162]
3. Horsman MR, Bohn AB, Busk M. Vascular targeting therapy: potential benefit depends on tumor and host related effects. Exp Oncol. 2010; 32(3):143–8. [PubMed: 21403608]
4. Horsman MR, Murata R. Combination of vascular targeting agents with thermal or radiation therapy. Int J Radiat Oncol Biol Phys. 2002; 54(5):1518–23. [PubMed: 12459380]
5. Chao BH, He X, Bischof JC. Pre-treatment inflammation induced by TNF-alpha augments cryosurgical injury on human prostate cancer. Cryobiology. 2004; 49(1):10–27. [PubMed: 15265713]
6. Balkwill F. Tumour necrosis factor and cancer. Nat Rev Cancer. 2009; 9(5):361–71. [PubMed: 19343034]
7. Rustin GJ, Galbraith SM, Anderson H, Stratford M, Folkes LK, Sena L, Gumbrell L, Price PM. Phase I clinical trial of weekly combretastatin A4 phosphate: clinical and pharmacokinetic results. J Clin Oncol. 2003; 21(15):2815–22. [PubMed: 12807934]
8. Dowlati A, Robertson K, Cooney M, Petros WP, Stratford M, Jesberger J, Rafie N, Overmoyer B, Makkar V, Stambler B, Taylor A, Waas J, Lewin JS, McCrae KR, Remick SC. A phase I pharmacokinetic and translational study of the novel vascular targeting agent combretastatin a-4 phosphate on a single-dose intravenous schedule in patients with advanced cancer. Cancer Res. 2002; 62(12):3408–16. [PubMed: 12067983]
9. Cooney MM, Radivoyevitch T, Dowlati A, Overmoyer B, Levitan N, Robertson K, Levine SL, DeCaro K, Buchter C, Taylor A, Stambler BS, Remick SC. Cardiovascular safety profile of combretastatin a4 phosphate in a single-dose phase I study in patients with advanced cancer. Clin Cancer Res. 2004; 10(1 Pt 1):96–100. [PubMed: 14734457]
10. Rustin GJ, Bradley C, Galbraith S, Stratford M, Loadman P, Waller S, Bellenger K, Gumbrell L, Folkes L, Halbert G. 5,6-dimethylxanthenone-4-acetic acid (DMXAA), a novel antivascular agent:

phase I clinical and pharmacokinetic study. Br J Cancer. 2003; 88(8):1160–7. [PubMed: 12698178]

11. Lejeune F, Lienard D, Eggermont A. Regional Administration of Recombinant Tumour Necrosis Factor-alpha in Cancer, with Special Reference to Melanoma. BioDrugs. 1998; 9(3):211–8. [PubMed: 18020561]
12. Grunhagen DJ, de Wilt JH, van Geel AN, Verhoef C, Eggermont AM. Isolated limb perfusion with TNF-alpha and melphalan in locally advanced soft tissue sarcomas of the extremities. Recent Results Cancer Res. 2009; 179:257–70. [PubMed: 19230545]
13. Libutti SK, Paciotti GF, Byrnes AA, Alexander HR, Gannon WE Jr, Walker M, Seidel GD, Yuldasheva N, Tamarkin L. Phase I and Pharmacokinetic Studies of CYT-6091; a Novel PEGylated Colloidal Gold-rhTNF Nanomedicine. Clin Cancer Res. 2010
14. Goel R, Swanlund D, Coad J, Paciotti GF, Bischof JC. TNF-{alpha}-based accentuation in cryoinjury--dose, delivery, and response. Mol Cancer Ther. 2007; 6(7):2039–2047. [PubMed: 17620433]
15. Jiang J, Goel R, Schmechel S, Vercellotti G, Forster C, Bischof J. PreConditioning Cryosurgery: Cellular and Molecular Mechanisms and Dynamics of TNF-alpha Enhanced Cryotherapy in an in vivo Prostate Cancer Model System. Cryobiology. 2010
16. Visaria RK, Griffin RJ, Williams BW, Ebbini ES, Paciotti GF, Song CW, Bischof JC. Enhancement of tumor thermal therapy using gold nanoparticle-assisted tumor necrosis factor-{alpha} delivery. Mol Cancer Ther. 2006; 5(4):1014–1020. [PubMed: 16648573]
17. Farma JM, Puhlmann M, Soriano PA, Cox D, Paciotti GF, Tamarkin L, Alexander HR. Direct evidence for rapid and selective induction of tumor neovascular permeability by tumor necrosis factor and a novel derivative, colloidal gold bound tumor necrosis factor. Int J Cancer. 2007; 120(11):2474–80. [PubMed: 17330231]
18. Bierhaus A, Zhang Y, Deng Y, Mackman N, Quehenberger P, Haase M, Luther T, Muller M, Bohrer H, Greten J, et al. Mechanism of the tumor necrosis factor alpha-mediated induction of endothelial tissue factor. J Biol Chem. 1995; 270(44):26419–32. [PubMed: 7592857]
19. Prinzen FW, Bassingthwaighte JB. Blood flow distributions by microsphere deposition methods. Cardiovasc Res. 2000; 45(1):13–21. [PubMed: 10728307]
20. Rosset A, Spadola L, Ratib O. OsiriX: an open-source software for navigating in multidimensional DICOM images. J Digit Imaging. 2004; 17(3):205–16. [PubMed: 15534753]
21. Daldrup HE, Shames DM, Husseini W, Wendland MF, Okuhata Y, Brasch RC. Quantification of the extraction fraction for gadopentetate across breast cancer capillaries. Magn Reson Med. 1998; 40(4):537–43. [PubMed: 9771570]
22. Deoni SC, Peters TM, Rutt BK. High-resolution T1 and T2 mapping of the brain in a clinically acceptable time with DESPOT1 and DESPOT2. Magn Reson Med. 2005; 53(1):237–41. [PubMed: 15690526]
23. Jiang J, Goel R, Iftekhar MA, Visaria R, Belcher JD, Vercellotti GM, Bischof JC. Tumor necrosis factor-{alpha}-induced accentuation in cryoinjury: mechanisms in vitro and in vivo. Mol Cancer Ther. 2008; 7(8):2547–2555. [PubMed: 18723499]
24. Jiang J, Bischof J. Effect of timing, dose and interstitial versus nanoparticle delivery of tumor necrosis factor alpha in combinatorial adjuvant cryosurgery treatment of ELT-3 uterine fibroid tumor. Cryo Letters. 2010; 31(1):50–62. [PubMed: 20309509]
25. Breitbach CJ, De Silva NS, Falls TJ, Aladl U, Evgin L, Paterson J, Sun YY, Roy DG, Rintoul JL, Daneshmand M, Parato K, Stanford MM, Lichty BD, Fenster A, Kirn D, Atkins H, Bell JC. Targeting tumor vasculature with an oncolytic virus. Mol Ther. 2011; 19(5):886–94. [PubMed: 21364541]
26. R Development Core Team. R: A language and environment for statistical computing. R Foundation for Statistical Computing; Vienna, Austria: 2011. URL http://www.R-project.org/
27. Visaria R, Bischof JC, Loren M, Williams B, Ebbini E, Paciotti G, Griffin R. Nanotherapeutics for enhancing thermal therapy of cancer. Int J Hyperthermia. 2007; 23(6):501–11. [PubMed: 17952764]

28. Spear MA, LoRusso P, Mita A, Mita M. Vascular disrupting agents (VDA) in oncology: advancing towards new therapeutic paradigms in the clinic. Curr Drug Targets. 2011; 12(14):2009–15. [PubMed: 21777190]
29. Heidel JD, Davis ME. Clinical developments in nanotechnology for cancer therapy. Pharm Res. 2011; 28(2):187–99. [PubMed: 20549313]
30. Shenoi MM, Shah NB, Griffin RJ, Vercellotti GM, Bischof JC. Nanoparticle preconditioning for enhanced thermal therapies in cancer. Nanomedicine. 2011; 6(3):545–563. [PubMed: 21542691]
31. Poon RTP, Borys N. Lyso-thermosensitive liposomal doxorubicin: an adjuvant to increase the cure rate of radiofrequency ablation in liver cancer. Future Oncology. 2011; 7(8):937–945. [PubMed: 21823888]
32. Perrault SD, Walkey C, Jennings T, Fischer HC, Chan WC. Mediating tumor targeting efficiency of nanoparticles through design. Nano Lett. 2009; 9(5):1909–15. [PubMed: 19344179]
33. Shah NB, Vercellotti GM, White JG, Bischof JC, Wagner CR, Fegan A. Blood-Nanoparticle Interactions and in Vivo Biodistribution: Impact of Surface Peg and Ligand Properties. Mol Pharm. 2012
34. Ferrero E, Zocchi MR, Magni E, Panzeri MC, Curnis F, Rugarli C, Ferrero ME, Corti A. Roles of tumor necrosis factor p55 and p75 receptors in TNF-alpha-induced vascular permeability. Am J Physiol Cell Physiol. 2001; 281(4):C1173–9. [PubMed: 11546653]
35. Siemann DW. The unique characteristics of tumor vasculature and preclinical evidence for its selective disruption by Tumor-Vascular Disrupting Agents. Cancer Treatment Reviews. 2010 In Press, Corrected Proof.
36. Nathan P, Zweifel M, Padhani AR, Koh DM, Ng M, Collins DJ, Harris A, Carden C, Smythe J, Fisher N, Taylor NJ, Stirling JJ, Lu SP, Leach MO, Rustin GJ, Judson I. Phase I Trial of Combretastatin A4 Phosphate (CA4P) in Combination with Bevacizumab in Patients with Advanced Cancer. Clin Cancer Res. 2012; 18(12):3428–39. [PubMed: 22645052]
37. Mukherjee P, Bhattacharya R, Wang P, Wang L, Basu S, Nagy JA, Atala A, Mukhopadhyay D, Soker S. Antiangiogenic properties of gold nanoparticles. Clin Cancer Res. 2005; 11(9):3530–4. [PubMed: 15867256]
38. Hoffmann NE, Bischof JC. Cryosurgery of normal and tumor tissue in the dorsal skin flap chamber: Part I--thermal response. J Biomech Eng. 2001; 123(4):301–9. [PubMed: 11563754]
39. Hoffmann NE, Bischof JC. Cryosurgery of normal and tumor tissue in the dorsal skin flap chamber: Part II--injury response. J Biomech Eng. 2001; 123(4):310–6. [PubMed: 11563755]
40. Bhowmick S, Hoffmann NE, Bischof JC. Thermal therapy of prostate tumor tissue in the dorsal skin flap chamber. Microvasc Res. 2002; 64(1):170–3. [PubMed: 12074643]
41. Bhowmick S, Coad JE, Swanlund DJ, Bischof JC. In vitro thermal therapy of AT-1 Dunning prostate tumours. Int J Hyperthermia. 2004; 20(1):73–92. [PubMed: 14612315]
42. Bischof JC, Smith D, Pazhayannur PV, Manivel C, Hulbert J, Roberts KP. Cryosurgery of dunning AT-1 rat prostate tumor: thermal, biophysical, and viability response at the cellular and tissue level. Cryobiology. 1997; 34(1):42–69. [PubMed: 9028916]
43. Fukumura D, Salehi HA, Witwer B, Tuma RF, Melder RJ, Jain RK. Tumor necrosis factor alpha-induced leukocyte adhesion in normal and tumor vessels: effect of tumor type, transplantation site, and host strain. Cancer Res. 1995; 55(21):4824–9. [PubMed: 7585514]
44. Mileski WJ, Raymond JF, Winn RK, Harlan JM, Rice CL. Inhibition of leukocyte adherence and aggregation for treatment of severe cold injury in rabbits. J Appl Physiol. 1993; 74(3):1432–6. [PubMed: 8482687]
45. Johansson A, Hamzah J, Payne CJ, Ganss R. Tumor-targeted TNFalpha stabilizes tumor vessels and enhances active immunotherapy. Proc Natl Acad Sci U S A. 2012; 109(20):7841–6. [PubMed: 22547817]
46. Thamm DH, Kurzman ID, Clark MA, Ehrhart EJ 3rd, Kraft SL, Gustafson DL, Vail DM. Preclinical investigation of PEGylated tumor necrosis factor alpha in dogs with spontaneous tumors: phase I evaluation. Clin Cancer Res. 2010; 16(5):1498–508. [PubMed: 20160058]
47. Tsunoda S, Ishikawa T, Yamamoto Y, Kamada H, Koizumi K, Matsui J, Tsutsumi Y, Hirano T, Mayumi T. Enhanced antitumor potency of polyethylene glycolylated tumor necrosis factor-alpha:

a novel polymer-conjugation technique with a reversible amino-protective reagent. J Pharmacol Exp Ther. 1999; 290(1):368–72. [PubMed: 10381801]

48. Tsutsumi Y, Tsunoda S, Kamada H, Kihira T, Nakagawa S, Kaneda Y, Kanamori T, Mayumi T. Molecular design of hybrid tumour necrosis factor-alpha. II: The molecular size of polyethylene glycol-modified tumour necrosis factor-alpha affects its anti-tumour potency. Br J Cancer. 1996; 74(7):1090–5. [PubMed: 8855980]
49. Yamamoto Y, Tsutsumi Y, Yoshioka Y, Nishibata T, Kobayashi K, Okamoto T, Mukai Y, Shimizu T, Nakagawa S, Nagata S, Mayumi T. Site-specific PEGylation of a lysine-deficient TNF-alpha with full bioactivity. Nat Biotechnol. 2003; 21(5):546–52. [PubMed: 12665803]
50. Yoshioka Y, Tsutsumi Y, Ikemizu S, Yamamoto Y, Shibata H, Nishibata T, Mukai Y, Okamoto T, Taniai M, Kawamura M, Abe Y, Nakagawa S, Nagata S, Yamagata Y, Mayumi T. Optimal site-specific PEGylation of mutant TNF-alpha improves its antitumor potency. Biochem Biophys Res Commun. 2004; 315(4):808–14. [PubMed: 14985084]
51. Kamada H, Tsutsumi Y, Yamamoto Y, Kihira T, Kaneda Y, Mu Y, Kodaira H, Tsunoda SI, Nakagawa S, Mayumi T. Antitumor activity of tumor necrosis factor-alpha conjugated with polyvinylpyrrolidone on solid tumors in mice. Cancer Res. 2000; 60(22):6416–20. [PubMed: 11103807]
52. Kaneda Y, Yamamoto Y, Kamada H, Tsunoda S, Tsutsumi Y, Hirano T, Mayumi T. Antitumor activity of tumor necrosis factor alpha conjugated with divinyl ether and maleic anhydride copolymer on solid tumors in mice. Cancer Res. 1998; 58(2):290–5. [PubMed: 9443407]
53. Tabata Y, Noda Y, Matsui Y, Ikada Y. Targeting of tumor necrosis factor to tumor by use of dextran and metal coordination. J Control Release. 1999; 59(2):187–96. [PubMed: 10332053]
54. Corti A, Ponzoni M. Tumor vascular targeting with tumor necrosis factor alpha and chemotherapeutic drugs. Ann N Y Acad Sci. 2004; 1028:104–12. [PubMed: 15650236]
55. Borsi L, Balza E, Carnemolla B, Sassi F, Castellani P, Berndt A, Kosmehl H, Biro A, Siri A, Orecchia P, Grassi J, Neri D, Zardi L. Selective targeted delivery of TNFalpha to tumor blood vessels. Blood. 2003; 102(13):4384–92. [PubMed: 12933583]
56. ten Hagen TL, Seynhaeve AL, van Tiel ST, Ruiter DJ, Eggermont AM. Pegylated liposomal tumor necrosis factor-alpha results in reduced toxicity and synergistic antitumor activity after systemic administration in combination with liposomal doxorubicin (Doxil) in soft tissue sarcoma-bearing rats. Int J Cancer. 2002; 97(1):115–20. [PubMed: 11774252]
57. Fang C, Shi B, Pei YY, Hong MH, Wu J, Chen HZ. In vivo tumor targeting of tumor necrosis factor-alpha-loaded stealth nanoparticles: effect of MePEG molecular weight and particle size. Eur J Pharm Sci. 2006; 27(1):27–36. [PubMed: 16150582]
58. Li YP, Pei YY, Zhou ZH, Zhang XY, Gu ZH, Ding J, Zhou JJ, Gao XJ, Zhu JH. Stealth polycyanoacrylate nanoparticles as tumor necrosis factor-alpha carriers: pharmacokinetics and anti-tumor effects. Biol Pharm Bull. 2001; 24(6):662–5. [PubMed: 11411555]
59. Arora A, Su G, Mathiowitz E, Reineke J, Chang AE, Sabel MS. Neoadjuvant intratumoral cytokine-loaded microspheres are superior to postoperative autologous cellular vaccines in generating systemic anti-tumor immunity. J Surg Oncol. 2006; 94(5):403–12. [PubMed: 16967445]
60. Sabel MS, Skitzki J, Stoolman L, Egilmez NK, Mathiowitz E, Bailey N, Chang WJ, Chang AE. Intratumoral IL-12 and TNF-alpha-loaded microspheres lead to regression of breast cancer and systemic antitumor immunity. Ann Surg Oncol. 2004; 11(2):147–56. [PubMed: 14761917]

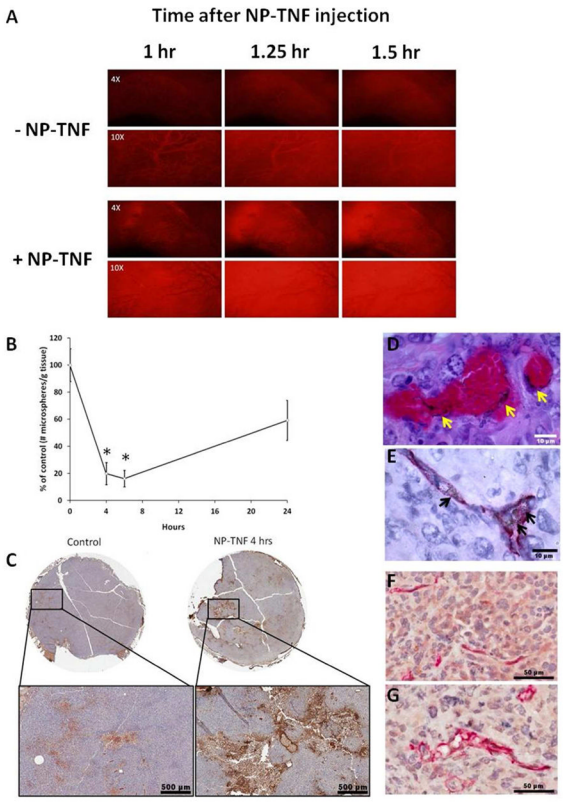

Figure 1.

Vascular effects of NP-TNF on LNCaP tumors. (A) Effect of NP-TNF on tumor vascular hyperpermeability. TxRed-labeled dextran was intravenously injected 1 hour after NP-TNF administration. (B) Microsphere accumulation data demonstrating the effect of NP-TNF pretreatment on hindlimb LNCaP tumor perfusion (*, $p < 0.01$, compared to 0 hours). Data presented as mean ± SE. (C) Fibrinogen stained sections of DSFC LNCaP tumors with and without NP-TNF pretreatment. Silver staining of (D) H&E section and (E) CD31-stained section of DSFC LNCaP tumors showing localization of NP-TNF to the tumor vasculature. Black areas/specks indicated by arrows are silver precipitates on the gold nanoparticles. CD31 stained sections of (F) control tumor and (G) NP-TNF treated tumor demonstrating increase in microvessel size of DSFC LNCaP tumors following NP-TNF treatment.

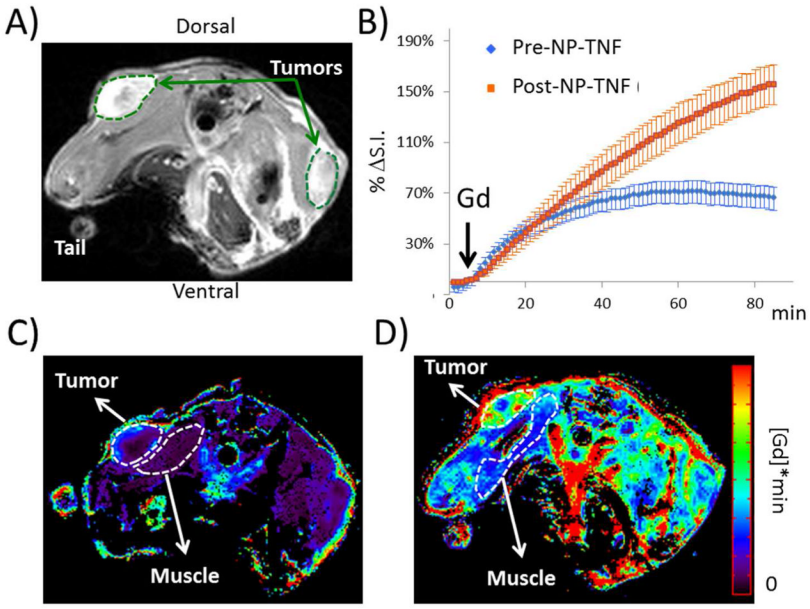

Figure 2.

Imaging vascular effects of NP-TNF using DCE-MRI. (A) Axial view of a mouse after NP-TNF and gadolinium injection. Representative tumor ROIs (broken green curves) used to generate the dynamic curves in (B) are shown for the two tumors in this example image. (B) Dynamic curves of the percent change in signal intensity (S.I.) over the time course of the DCE-MRI acquisition obtained in all tumors (n=10) before and after NP-TNF administration (mean ± SEM). AUGC maps from Pre-NP-TNF (C) and Post-NP-TNF (D) experiments are shown from the same mouse. The tumor and muscle ROIs (broken white curves) in (C) and (D) show regions used to compare contrast accumulation. The muscle ROIs are noticeably different as there were unavoidable variations in animal positioning between the two studies which were several days apart. The muscle regions needed to be drawn avoiding major vessels and bone in each case.

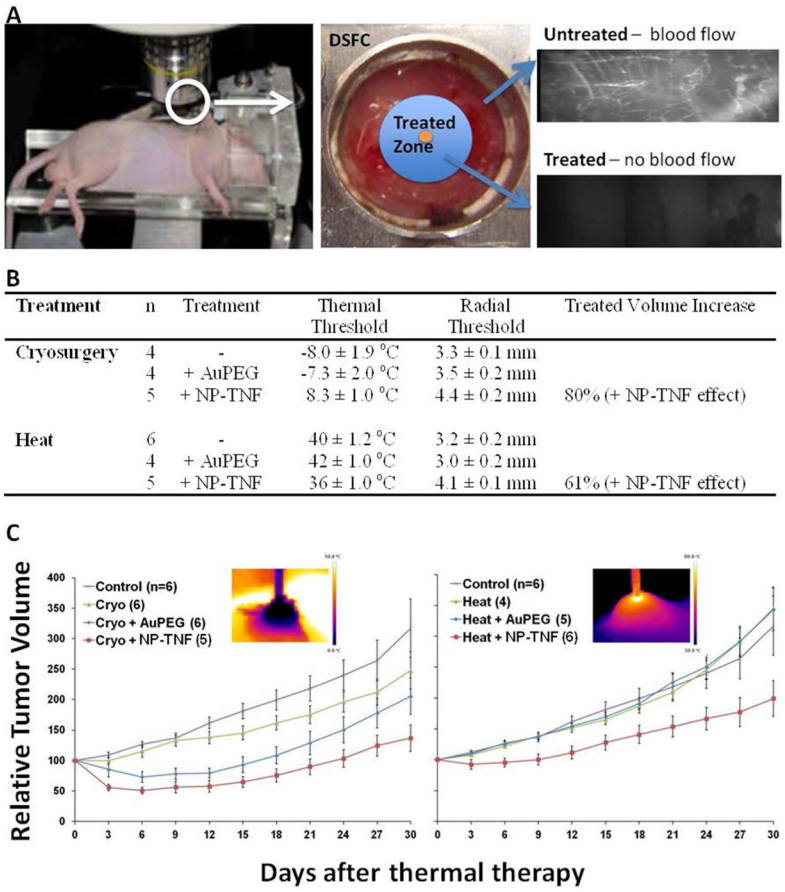

Treatment	n	Treatment	Thermal Threshold	Radial Threshold	Treated Volume Increase
Cryosurgery	4	-	-8.0 ± 1.9 °C	3.3 ± 0.1 mm	
	4	+ AuPEG	-7.3 ± 2.0 °C	3.5 ± 0.2 mm	
	5	+ NP-TNF	8.3 ± 1.0 °C	4.4 ± 0.2 mm	80% (+ NP-TNF effect)
Heat	6	-	40 ± 1.2 °C	3.2 ± 0.2 mm	
	4	+ AuPEG	42 ± 1.0 °C	3.0 ± 0.2 mm	
	5	+ NP-TNF	36 ± 1.0 °C	4.1 ± 0.1 mm	61% (+ NP-TNF effect)

Figure 3.

Multimodal cancer therapy using NP-TNF. (A) Schematic depicting the DSFC tumor model and assessment of vascular stasis following thermal therapy. (B) Thermal and vascular stasis (radial) thresholds obtained following thermal therapy with and without nanoparticle pretreatment in LNCaP DSFC tumors. Data are mean ± SEM. (C) Tumor growth delay following thermal therapy with and without nanoparticle pretreatment in hindlimb LNCaP tumor model. Insets depict infrared images obtained during thermal therapy. Data are mean ± SEM.

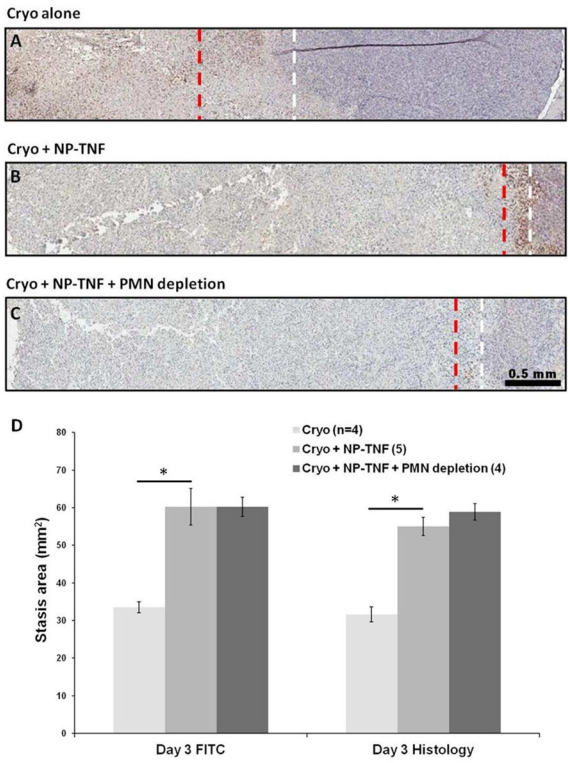

Figure 4.

NP-TNF and acute inflammatory response. Myeloperoxidase (MPO) stained DSFC sections following (A) Cryosurgery only, (B) Cryosurgery + NP-TNF, and (C) Cryosurgery + NP-TNF after systemic neutrophil depletion. The red dashed line indicates the prominent edge of the inflammatory band. The white dashed line indicates the edge of viable tumor. (D) Comparison of Day 3 stasis areas measured by vascular imaging (FITC) and histology of the three groups (*, $p < 0.05$). Data are mean ± SEM.

Table 1

Strategies for tumor selective delivery of TNF-α.

Delivery method	Sub-type	Stage of development	Tumor	Outcome measure	Reference
Polymer conjugation	Polyethylene glycol	Preclinical	Spontaneous tumors (dog) Meth-A fibrosarcoma (mouse) Sarcoma-180 (mouse) Meth-A fibrosarcoma (mouse) Meth-A fibrosarcoma (mouse)	Tumor growth, tumor necrosis Tumor necrosis Tumor growth, tumor necrosis Tumor necrosis Tumor necrosis	Thamm et al. [46] Tsunoda et al. [47] Tsutsumi et al. [48] Yamamoto et al. [49] Yoshioka et al.[50]
	Polyvinylpyrrolidone	Preclinical	Meth-A fibrosarcoma (mouse)	Tumor growth, survival time	Kamada et al. [51]
	Divinyl ether-maleic anhydride copolymer	Preclinical	Meth-A fibrosarcoma (mouse)	Tumor growth, tumor necrosis, survival time	Kaneda et al. [52]
	Dextran	Preclinical	Meth-A fibrosarcoma (mouse)	Tumor growth	Tabata et al. [53]
Peptide conjugation	CNGRC peptide	Phase II	Mesothelioma	Progression free survival (in progress)	Corti and Ponzoni [54]
	RGR peptide	Preclinical	Pancreatic neuroendocrine (mouse)	Immune response, survival time	Johansson et al. [45]
Antibody conjugation	Antibody fragment to extradomain B of fibronectin	Preclinical	F9 embryonal teratocarcinoma (mouse)	Tumor growth, tumor cell viability	Borsi et al. [55]
Metallic Nanoparticle	Colloidal gold	Phase I	Advanced solid organ tumors (human)	Dose limiting toxicity, adverse events	Libutti et al. [13]
Liposomal Nanoparticle	PEG-conjugated phosphatidylcholine	Preclinical	BN-175 sarcoma (mouse)	Tumor growth, tumor necrosis, response rate	ten Hagen et al. [56]
Polymeric Nanoparticle	PEG-conjugated cyanoacrylate-co-n-hexadecyl cyanoacrylate	Preclinical	Sarcoma-180 (mouse)	Tumor growth	Li et al. [58]
Microspheres	Polylactic acid	Preclinical	B16 melanoma (mouse) MT-901 carcinoma (mouse)	Tumor volume, survival time Tumor volume, survival time	Arora et al. [59] Sabel et al. [60]